AD-A050 212 GEORGIA INST OF TECH ATLANTA SCHOOL OF PHYSICS F/G 11/6
OPTICAL SURFACE STUDIES OF TITANIUM AND TITANIUM-ALUMINUM ALLOY--ETC(U)
NOV 77 J R STEVENSON AFOSR-75-2773

UNCLASSIFIED AFOSR-TR-78-0079 NL

1 OF 1
AD
A050 212

END
DATE
FILMED
3-78
DDC

AFOSR-TR- 78-0079

AD A050212

AD No. ____
DDC FILE COPY

(2)

DDC
RECEIVED
FEB 21 1978
B

DISTRIBUTION STATEMENT A
Approved for public release;
Distribution Unlimited

UNCLASSIFIED
SECURITY CLASSIFICATION OF THIS PAGE (When Data Entered)

REPORT DOCUMENTATION PAGE

READ INSTRUCTIONS BEFORE COMPLETING FORM

1. REPORT NUMBER: AFOSR-TR- 78-0079
2. GOVT ACCESSION NO.
3. RECIPIENT'S CATALOG NUMBER
(9) Final rept. 1 Jul 75-30 Sep 77

4. TITLE (and Subtitle): (6) Optical Surface Studies Of Titanium And Titanium-Aluminum Alloys With Application To The Mechanism Of Passivity And Non-Destructive Testing
5. TYPE OF REPORT & PERIOD COVERED: July 1, 1975 to Sept. 30, 1977 FINAL
6. PERFORMING ORG. REPORT NUMBER

7. AUTHOR(s): (10) JAMES R. STEVENSON
8. CONTRACT OR GRANT NUMBER(s): (15) AFOSR 75-2773

9. PERFORMING ORGANIZATION NAME AND ADDRESS: GEORGIA INSTITUTE OF TECHNOLOGY, SCHOOL OF PHYSICS, ATLANTA, GA 30332
10. PROGRAM ELEMENT, PROJECT, TASK AREA & WORK UNIT NUMBERS: (26) 2306A2, 61102F (17) A2

11. CONTROLLING OFFICE NAME AND ADDRESS: AIR FORCE OFFICE OF SCIENTIFIC RESEARCH/NE, BOLLING AFB, BUILDING 410, WASHINGTON, DC 20332
12. REPORT DATE: Nov. 15, 1977 (11) 15 Nov 77
13. NUMBER OF PAGES: 44 (12) 48p.

14. MONITORING AGENCY NAME & ADDRESS (if different from Controlling Office): (18) AFOSR (19) TR-78-0079
15. SECURITY CLASS.: UNCLASSIFED
15a. DECLASSIFICATION/DOWNGRADING SCHEDULE

16. DISTRIBUTION STATEMENT (of this Report)

APPROVED FOR PUBLIC RELEASE; DISTRIBUTION UNLIMITED

17. DISTRIBUTION STATEMENT (of the abstract entered in Block 20, if different from Report)

18. SUPPLEMENTARY NOTES

19. KEY WORDS (Continue on reverse side if necessary and identify by block number)

REFLECTANCE, METALS, ALLOYS, SYNCHROTRON RADIATION, AUGER

20. ABSTRACT (Continue on reverse side if necessary and identify by block number)

Optical reflectance studies and Auger spectroscopy have been used to study Ti and Ti-Al alloy surfaces to study mechanisms relative to the formation of of passive surfaces. Instrumentation has been developed for rapid data acquisition so that growth kinetics of oxide formation on the surface can be followed with non-destructive optical techniques. The use of synchrotron radiation has been an important tool in the surface studies. The measured optical reflectivity of titanium and titanium-aluminum are discussed in the light of new theoretical calculations. New theoretical methods in the analysis of

DD FORM 1 JAN 73 1473 EDITION OF 1 NOV 65 IS OBSOLETE

404 227 JOB

UNCLASSIFIED
SECURITY CLASSIFICATION OF THIS PAGE (When Data Entered)

20.

Auger data has resulted in a significant improvement of information about the chemical environment of the surface.

Final Scientific Report

Optical Surface Studies of Titanium and Titanium-Aluminum Alloys with Application to the Mechanism of Passivity and Non-Destructive Testing

James R. Stevenson

November 15, 1977

Grant No. AFOSR 75-2773

This research was supported by the Air Force Office of Scientific Research (AFSC) under grant No. AFOSR 75-2773.

Qualified requestors may obtain additional copies from the Defense Documentation center. All others should apply to the Clearinghouse for Federal Scientific and Technical Information.

I. Objectives

The purpose of this research was to study the optical properties of titanium and titanium-aluminum surfaces. These surfaces were to be studied as oxides were formed on the surface and through an analysis of optical reflectivity data and Auger electron spectroscopy, some information regarding the chemistry of the oxide surface was to be sought. By comparison of clean surface optical reflectivity and oxide surface data, particular regions of optical sensitivity were to be identified which might lead to applications in the area of non-destructive testing.

II. Achievements

Progress has been achieved in a number of the objectives described above. In addition some scientific by-products of the research are described which may result in important contributions to the scientific community. The achievements below are preceeded by a summary sentence followed by a more detailed description.

A) Instrumentation Development

The necessity to follow oxide formation in situ led to the development of an ultrahigh vacuum chamber with provision for on-line optical and Auger data acquisition.

An automated surface analysis apparatus has been developed for optical and Auger studies of both clean and contaminated surfaces. The apparatus consists of an ultrahigh vacuum sample chamber/reflectometer equipped with a cylindrical mirror electron analyzer and various capabilities for surface cleaning and treatment, and a minicomputer with associated electronics for fast collection and display of data. The principle motivation for developing this apparatus was the need to make optical measurements of a surface well characterized by Auger spectroscopy to insure that an accurate correlation of the data can be made. When working with reactive surfaces, large changes can take place even at ultrahigh vacuum in a matter of seconds, requiring near simultaneous measurements.

The system has been developed so that three different types of data may be collected independently on the same sample with minimum mutual interference: Reflectance, Auger spectra (or photoemission) and ellipsometry data. The ultrahigh vacuum ion pumped sample chamber (see Figure 1) is designed such that all measurements and surface treatments may be performed with only minimal sample repositioning, allowing the maximum benefits from the high speed automated measurements. The chamber incorporates, in addition to the equipment for the three types of experimental spectroscopy, a liquid nitrogen cooled titanium sublimation pump to minimize the active residual gases in the system; a scanning ion gun for surface cleaning and bombardment with active gases; a gas manifold system that allows controlled amounts of both inert and active gases to be admitted to the system; an ion pressure guage; and a residual gas analyzer. The sample is mounted on a Varian sample manipulator, allowing accurate positioning of the sample. An electron bombardment sample heater and thermocouple are incorporated in the sample mount. Figure 2 shows schematically the instrumentation available within the sample chamber. All spectroscopy equipment is operated by a DEC PDP-8/L minicomputer using in-house designed and constructed

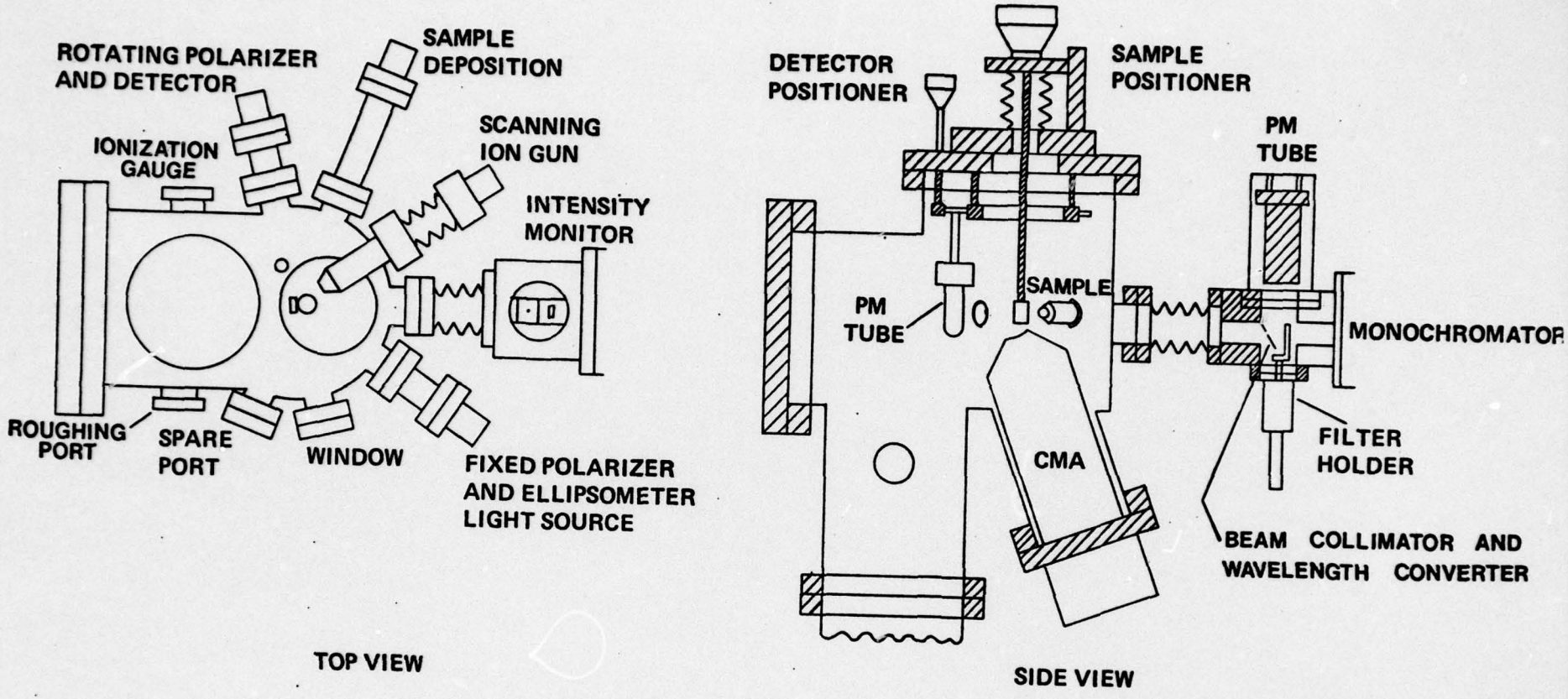

Figure 1 Schematic Diagram of Ultrahigh Vacuum Ion Pumped Sample Chamber

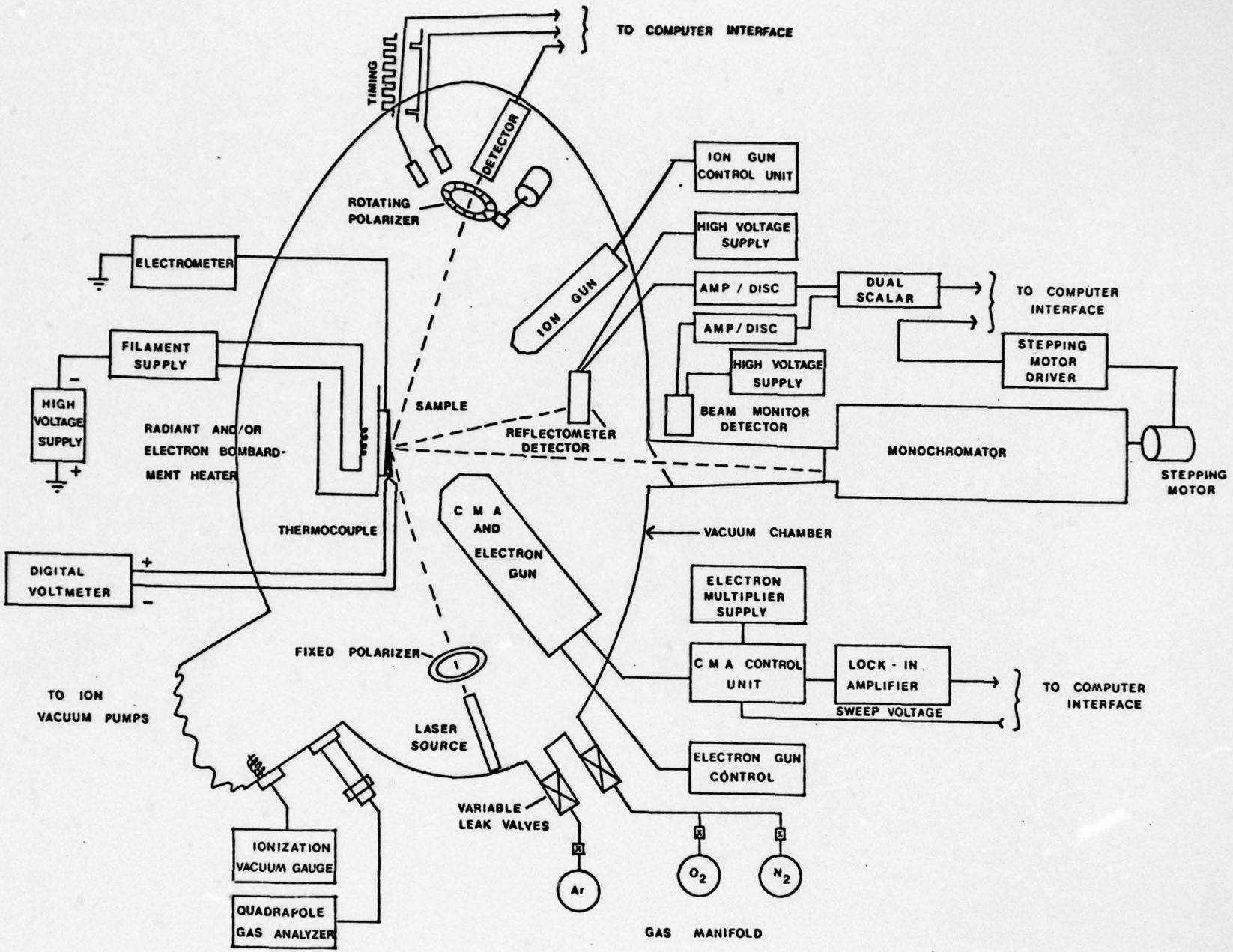

Figure 2 Instrumentation configuration in Ultrahigh Vacuum Sample Chamber

interfaces as shown in Figure 3. The PDP-8/L has a limited memory of 8K, necessitating the development of the control program in assembly language in order to conserve memory for both the program and data storage. Figure 4 illustrates how the control program is written in modular form allowing easy program modification. The system is task oriented, completely command initiated, and device interrupt driven. All idle time is used for the scope display. A flexible command decoder initiates all data collection and processing routines. If routines do not interfere with each other, more than one routine may be active at any time.

Reflectance (or transmission) measurements are made with a movable photomultiplier (PM) tube that is located inside the ultrahigh vacuum sample chamber. The PM tube is replaced by a channeltron detector for the VUV region of the spectrum. Light from a monochromator driven by a stepping motor passes into an intensity monitor chamber where part of the beam is collimated by a small aperture in a phosphor coated diaphram, passing into the sample chamber. The blocked portion of the beam is wavelength shifted by the phosphor and collected by a PM tube, yielding a measurement of the relative intensity of the beam. Suitable filters may be inserted in the beam in the monitor chamber to minimize second order effects. Both conventional discharge lamps and synchrotron radiation are used as a light source. When using a conventional source a lithium flouride window is placed between the monochromator and sample chamber to preserve the ultrahigh vacuum of the chamber, thus limiting measurements to an upper limit of eleven electron volts. The ultrahigh vacuum nature of a synchrotron source allows the entire system to operate at ultrahigh vacuum without windows, allowing measurements to 30eV or more depending on monochromator efficiency.

Both the beam monitor PM tube and the movable PM tube are operated in the single photon counting mode. Outputs from the PM tubes are fed to separate amplifier/discriminators having response times of less than 10 nsec; the outputs

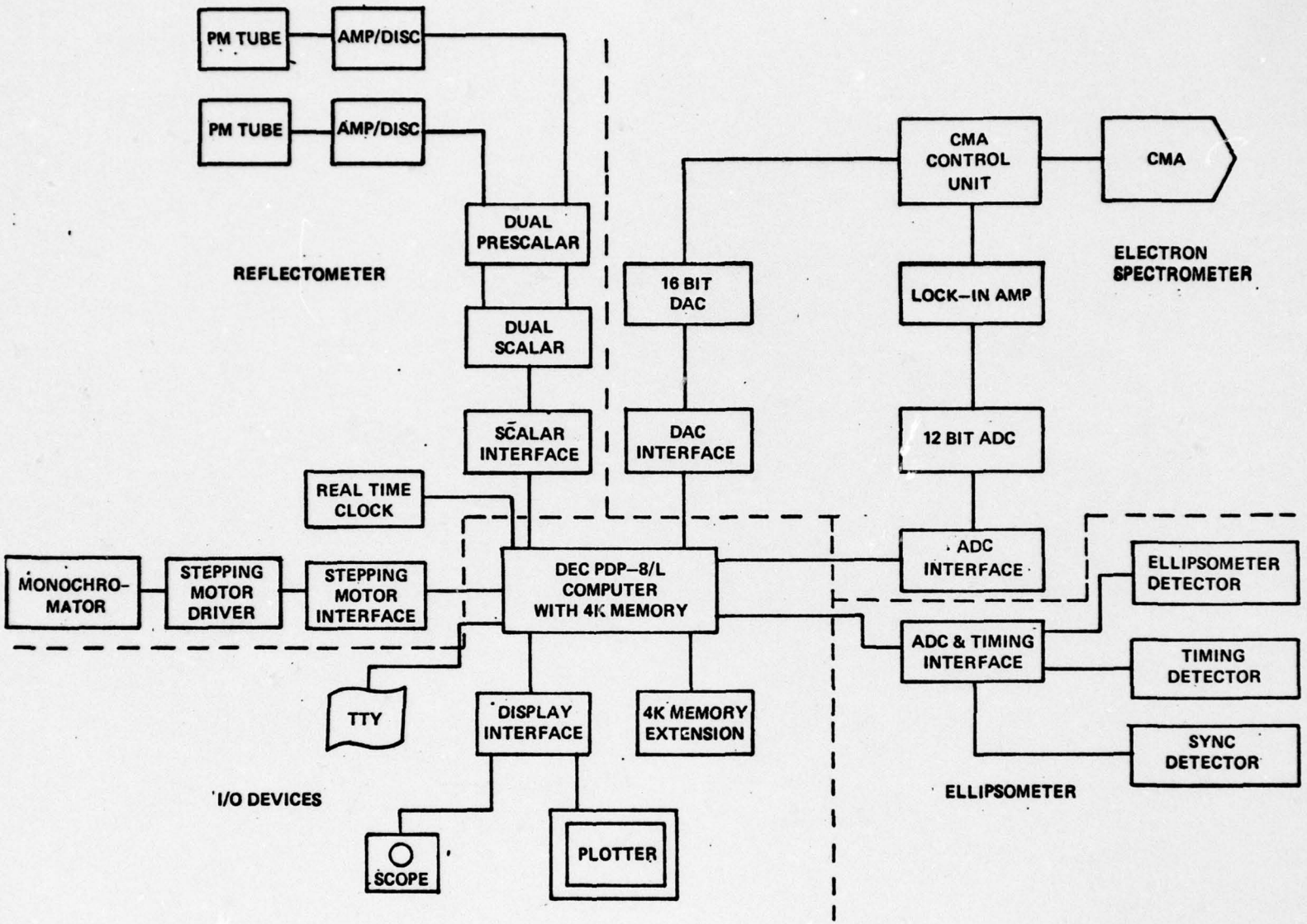

Figure 3 ELECTRONIC HARDWARE CONFIGURATION

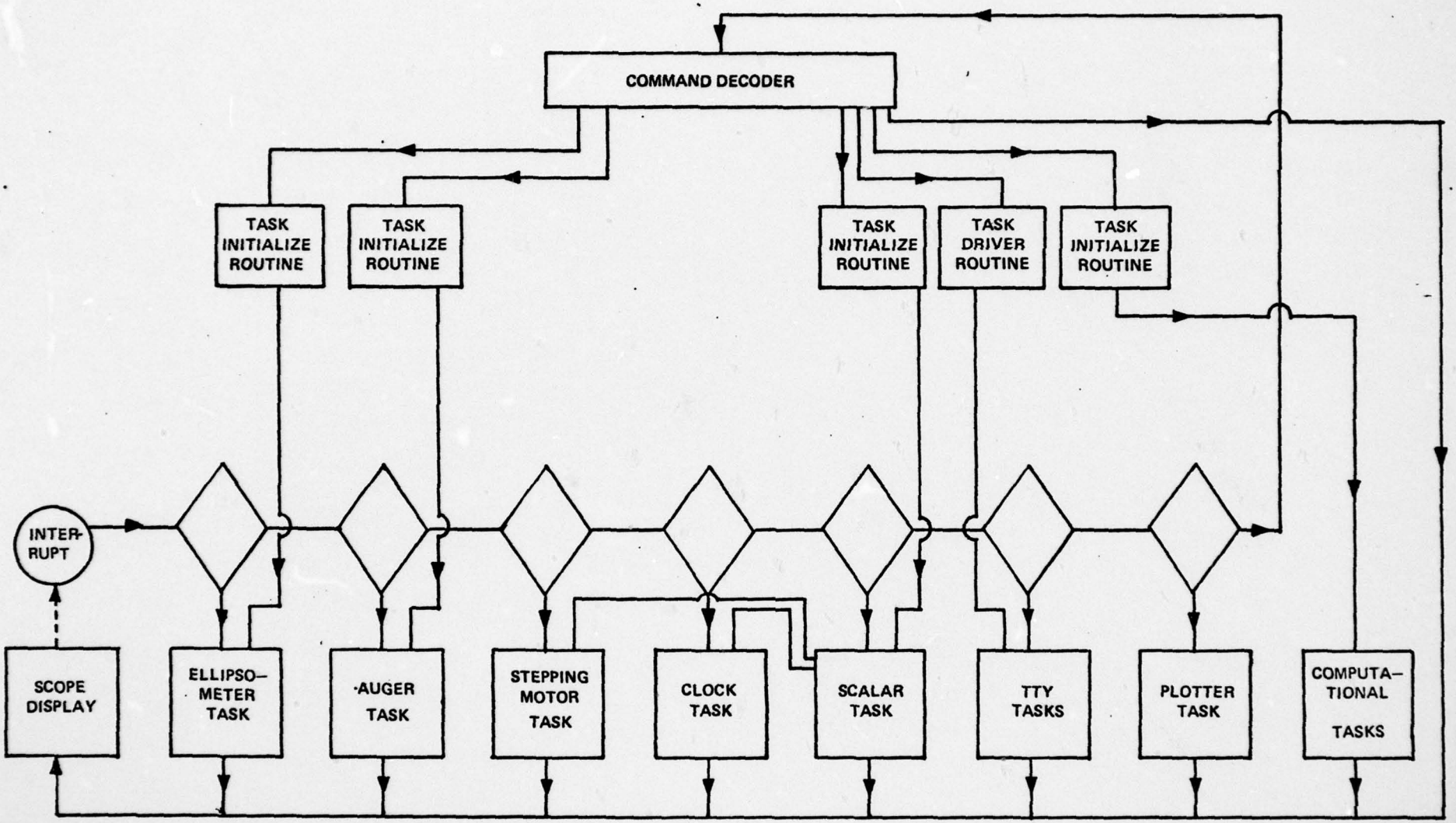

Figure 4 SIMPLIFIED PROGRAM FLOW CHART

of the discriminators drive decade prescalers which in turn feed a preset dual scalar having a response time of less than 100 nsec. This arrangement allows counting rates of a megahertz without serious non linearity due to pulse overlap. Dark count rates for the PM tubes are typically 100 Hz, resulting in a dynamic range of 40 db in the measurement process.

A typical measurement sequence would consist of the control program calculating a new position for the monochromator and executing the move; resetting and enabling the scalars; resetting and enabling the real time clock; finally entering the wait mode. When either of the scalars reach a preset maximum, both scalars are disabled, the clock is disabled and the scalars and clock are read. The time from the clock is multiplied by a previously measured average dark count rate for each PM tube; and the resulting values are subtracted from the appropriate count. The ratio of the noise corrected values is then computed and stored for further processing.

A reflectance spectrum is measured by first moving the sample from the beam and rotating the PM tube until it intercepts the beam. Using the appropriate "incident run" command, the response ratios of the two PM tubes for each data point are stored in one of four memory arrays. The sample is then aligned in the beam and the PM tube rotated to intercept the reflected beam. The PM tube is rotated about the sample such that the beam path length is the same for incidence and reflectance measurements. The appropriate "reflectance run" command measures the combined sample reflectance and PM tube response ratio and then calculates the ratio of this value with the value stored during the incidence run, yielding for each data point the sample reflectance.

as given by the following relationship:

$$\text{Reflectance} = \left[\frac{B_R - T_R B_N}{A_R - T_R A_N}\right] \Bigg/ \left[\frac{B_I - T_I B_N}{A_I - T_I A_N}\right] \qquad (1)$$

where A = count from scalar A

B= count from scalar B

T = time period count was accumulating

R = reflectance measurement

I = incident measurement

N = noise measurement

For both Auger electron spectroscopy and photoemission studies a PHI cylindrical mirror analyzer (CMA) is used without modification. Selection of the desired passband energy is accomplished by the application of a control voltage to the multiplex input of the CMA control unit. The control voltage is generated by a 16 bit digital to analog converter, yielding a smallest step of less than 0.1 eV, which is adequate resolution for both Auger and photoemission studies. The CMA is operated in its normal differential mode, using synchronous detection of the output. The detector output is digitized by means of a 12 bit ADC.

The control program allows up to seven energy windows to be scanned. The width of each window is an input parameter, determining the resolution of the data, since each window has a fixed number (64) of data points. The system may also be used in a "windowless" mode producing a continuous spectrum of 512 data points. Scanning takes place at a constant rate of 1000 data points per second allowing 1 nsec for recovery of the DAC and associated electronics. Windows are scanned sequentially; after scanning all windows the process is repeated, continually averaging the current data with the previous data.

using the following relationship:

$$\bar{X}_i = \frac{(i-1)\,\bar{X}_{i-1} + X_i}{i}$$

where X_i = ith measurement

$\bar{X}_i$ = average value after ith measurement

$\bar{X}_{i-1}$ = average value after (i-1)th measurement

An averaging period of 20 sweeps (approximately 10 seconds) produces data of good quality which is not significantly improved by further averaging.

Subsequent to data collection, peak-to-peak amplitude of the Auger transitions within each window may be calculated on command. For any given transition peak-to-peak height will be proportional to elemental concentration. When operating in depth profile mode a complete data collection routine will occur followed by the calculation and printing of peak-to-peak heights for each window. The system then waits for a specified length of time and repeats the process. If the sample is being simultaneously sputtered at a constant rate than the results are a printout of relative elemental concentration versus depth.

In Auger applications and, if sufficient intensity exists, in photoemission applications data is collected as the differential of the number of electrons versus energy. If direct electron distribution curves are needed, a quadrature routine will numerically integrate the data and display the result. A slightly modified equipment configuration allows the collection of photoemission electron distribution curves directly using electron counting. In this configuration the output of the CMA electron multiplier feeds an amplifier/discriminator, which inputs into the dual scalar. The other half of the scalar counts a 1 MHZ timing signal. Since both CMA energy and photon energy are under computer control, data may be collected and displayed in a variety of modes: photon energy fixed and analyzer energy varied, analyzer energy fixed and photon energy varied, or photon and analyzer energy varied synchronously, with constant

energy difference.

Ellipsometry Mode

The ellipsometer is designed as an ultrahigh vacuum compatible infrared system using a laser source. The beam from the laser passes through a fixed wire grid polarizer into the sample chamber, striking the sample at 70^{o} angle of incidence; exits the chamber, passing through a rotating polarizer and is detected by a pyroelectric detector. Rotating at approximately 600 rpm, the polarizer modulates the light intensity at the detector. Using a fast ADC, the output of the detector is measured 64 times for each revolution of the polarizer timing signals generated photoelectrically from timing marks on the mounting collar of the polarizer provide accurate correlation between detector output and polarizer position.

The resulting data from the ADC is partially Fourier analyzed by the PDP-8/L to determine the parameters of the ellipse. Fast analysis is accomplished by the use of stored cosine and sine look up tables and calculation of only the three needed Fourier coefficients rather than a full analysis. Averaging the data over a ten second period reduces the effective noise to less than the least significant bit of the ADC. Determination of the optical constants from the ellipse parameters is done off line.

B) Theoretical and Analytical Developments

Important contributions have resulted from theoretical efforts to extract both chemical and physical information from the optical and Auger spectroscopy data. Both refinement of existing techniques as well as introduction of new analytical procedures are described.

1. Refinement of techniques for obtaining optical constants from reflectance data- We have reduced the uncertainty in the Kramer-Kronig (KK) analysis of reflectance data in a finite energy range by adjusting the high energy

tail of the spectrum so that the density satisfies certain exact sum rules. Calculations show that the use of the density sum rule[1]

$$\int_0^\infty (n-1)\ \omega d\omega = 0 \qquad (2)$$

in addition to

$$\int_0^\infty (n-1)\ d\omega = 0 \qquad (3)$$

which is normally used alone in data analysis, greatly improves the accuracy of the KK analysis procedure. We have also found that comparisons between the sum rules are good checks for the consistency of our experimental data. In addition we are now using ellipsometric measurements taken at selected frequencies to improve our analysis. With these procedures we are able to obtain accurate spectra for the optical constants and to provide a measure of the uncertainty in the optical data.

2. Analysis of the optical constants to separate the effects of film and substrate- We have developed methods to derive film and substrate optical constants from the effective optical constants obtained by KK analysis. A computer analysis is used to obtain the film optical constants via a non-linear least square fit to the Fresnel equations upon inputting the known substrate optical constants and the film thickness. The film thinkness can be found independently from ellipsometric measurements. Our analysis shows quite often the film thickness need not be known to otain an accurate spectral shape for the optical constants as long as a reasonable range for the thickness can be assumed.

3. Development of techniques for obtaining several optical constants from ellipsometric data - We have generalized the usual McCrackin method for analyzing ellipsometric data by instituting a non-linear least square fitting procedure. With this method we can obtain consistent sets of substrate and film optical constants and film thicknesses from multiple angle of incidence and multiple film thickness measurements. The procedure has been automated so that sets of characteristic curves for thickness versus film and substrate optical constants are quickly generated. The intersections of these curves provide consistent sets of optical constants and thicknesses for given sets of ellipsometric data. This method is especially useful in checking whether the variation of one parameter (eg, film thickness) causes a much greater change in the characteristic curves than the variation of another parameter does.[3] Then analysis based on the former variation will be much less affected by experimental uncertainty.

4. Development of a method for analyzing Auger and photonelectron line shapes -

We have developed a method of analysis which is well suited to our higher resolution AES and ARPS experimental techniques. In this method the the experimental peaks are assumed to be composed of convolutions of known functions. We obtain the best fit to the individual peaks, the secondary electron background structure, and the inelastic loss structure using a non-linear least squares fitting procedure. Because the entire peak shape is used in the procedure, the linewidths, peak heights, and energy positions of even partially overlapped peaks can be determined to an accuracy an order of magnitude better than the instrument resolution.[4] Even for peaks that are weakly resolved, our method determines the energy positions accurately and gives somewhat less

accurate values for the linewidths and heights. The method is also flexible enough to allow, before the fitting procedure is undertaken, deconvolution of structure that cannot easily be fitted with simple functions. For example, the instrument resolution function is sometimes skewed, and the elastic scattering peak, which can be used to represent the resolution function when the secondary background and inelastic loss structure is removed, can then be deconvoluted from the data before the fitting.

Our method allows the extraction of the maximum amount of information from the photoelectron and Auger spectra in a way that can most easily be related to theoretical calculations.

5. Initiation of a program for analyzing chemical effects and surface bonding effects in the Auger and photoelectron spectra- We have taken the information from the above analysis of Auger and photoelectron lineshapes and peak energies, and we have obtained details of the core electron chemical shifts and the valence electron bonding structures. A qualitative theoretical analysis of the data yields information useful in identifying the chemical environment at a particular stage of oxidation and the likely bonding patterns. Our more complete calculations described below then are used to substantiate these identifications. This analysis provides a useful addition to the analysis of the optical data and highlights especially the changes in surface chemistry as the oxidation proceeds.

6. Undertaking of a series of SCF calculations for Ti-O systems to determine bonding and the effects of different configurations on core electron states. This program is quite valuable used in conjunction with the above analysis of Auger and photoelectron data. The calculated changes in bonding for different Ti-O systmes give insight into the changes occuring in core-valence Auger structure and in photoelectron valence structure. The calculated energy shifts of the core states are useful in identifying the chemical environments responsible

for the observed core chemical shifts in the electron spectra.

The computer codes obtained for these calculations and modified for use on our computer system are the most advanced available for ab-initio self-consistent field cluster calculations. They contain a core replacement option[5] which is invaluable when clusters containing heavier atoms are considered. The more precise description afforded by these codes to the interaction of an electron with the self-consistent field produced by the other electrons is sometimes necessary to obtain the correct bonding configurations.[6]

7. Undertaking of a series of calculations of oxide optical spectra based on accurate ab-initio band structure results- We have used the method of Mickish and Kunz[5] to develop a scheme for calculating the optical absorption spectrum. The contributions of the joint density of states and the oscillator strengths are included and some of the effects of the interaction of the excited electron with its hole are assessed. We have used our method on the energy bands for TiO calculated by Jennison and Kunz.[6] The calculated joint density of states and optical absorption show structure in general agreement with our optical absorption data. Using these results we have been able to assign the experimental structures to excitations between certain regions of particular energy bands. Since orbitals of a particular symmetry sometimes dominate these excitations, this information is quite useful for analyzing the changes the spectral structures undergo as the titanium oxidation proceeds. The orbital information is also useful in assessing the effects of particle-hole interactions which may shift some of the theoretical peaks significantly.

C) Experimental Measurements

Both optical reflectivity and Auger spectroscopy experimental results are reported for clean surfaces of titanium and titanium-aluminum alloy as well as oxidized surfaces. Results indicate that data in the scientific literature on the reflectivity of titanium is in error because of oxide contamination.

Samples were prepared for the experiment by mechanical polishing followed by electropolishing. After mounting the samples in the vacuum system, the entire system was baked at approximately 200°C. Using a combination of ion pumping and titanium sublimation on a cryogenic surface, the base pressure of the system was reduced to approximately 10^{-10} T. Prior to measurement of the reflectivity, the sample surface was characterized by Auger electron spectroscopy (AES). Reflectivity was measured for photons ranging in energy from 2 eV to 25 eV. In some cases this was extended to 40 eV. After measurement of the initial surface, the sample was bombarded with Ar ions to remove the oxides from the surface. After the Ar bombardment, the sample was then characterized by AES and reflectivity measurements. The process was repeated until no further changes were noted in either the Auger or reflectivity spectra. This was the "cleanest" surface. At this point controlled amounts of the reactive gas (oxygen or nitrogen) were admitted to the system, and after a measured exposure, flushed from the system. AES and reflectivity data were taken. This procedure was repeated several times, increasing exposure. Subsequently the surface was bombarded with the reactive gas ions and the measurements made as before. This procedure was also repeated with increasing bombardment times. Finally the process was reversed again, cleaning the surface with Ar ionsuntil the "clean" surface data could be reproduced.

1. Titanium-titanium oxide systems-

In Figure 5 we compare the reflectance spectra for the clean and oxidized titanium surfaces. We attribute the structures below 7 eV to transitions


TITANIUM
CLEAN SURFACE
OXIDIZED SURFACE
INITIAL SURFACE
REFLECTANCE
0
2
5
10
15
20
25
ENERGY (EV)
0
0
0

Figure 5

within the d-band region although there is undoubtedly some s and p mixing in these bands. This interpretation is consistent with that of Lynch et al,[7] and also with Ti $L_{II,III}$ x-ray emission and absorption data[8] which give an indication of the shapes and relative energy positions of the valence and conduction bands, respectively. We attribute the peak around 10 eV and the structure beyond 20 eV in the oxidized and initial surface spectra to transitions from the oxygen 2p and 2s bands, respectively. This interpretation is substantiated by the calculations of the joint density of states for the oxides[8] which indicate transitions involving the 2p and 2s bands should occur at these energies. In addition, the separation of 16 eV between the two peaks in the initial surface spectrum is just the free-atom value and has been seen in the XPS spectrum of TiO_2.[9] It is to be noted that these two peaks move to lower energy in the initial surface spectrum compared to the oxide spectrum. We believe the spectra differ because a TiO-like phase exists on the oxidized surface whereas a reduced TiO_2 exists on the initial surface. Our viewpoint is corroborated by the Auger data which show an oxygen peak-to-peak height twice as large for the initial surface as for the oxidized surface. The x-ray emission and absorption data also show a decrease in the separation of the oxygen 2p bands and the conduction bands in going from TiO to TiO_2.[8] In addition, there is a reduction in the height of the d-band structure between 5-7 eV relative to the oxygen 2p band in the initial surface reflectance as compared to the oxidized surface. Reduced TiO_2 should have a much lower occupation in the d-band region than TiO so that the reflectance structure due to these bands should be much less for TiO_2 than TiO.

For comparison we present the spectrum of Lynch et al[7] and our cleanest surface spectrum in Figure 6. The peaks around 10 eV and 25 eV appearing in Lynch's data disappear in ours, although a shoulder at about 13 eV remains. The Lynch spectrum falls somewhere between our initial surface and oxidized

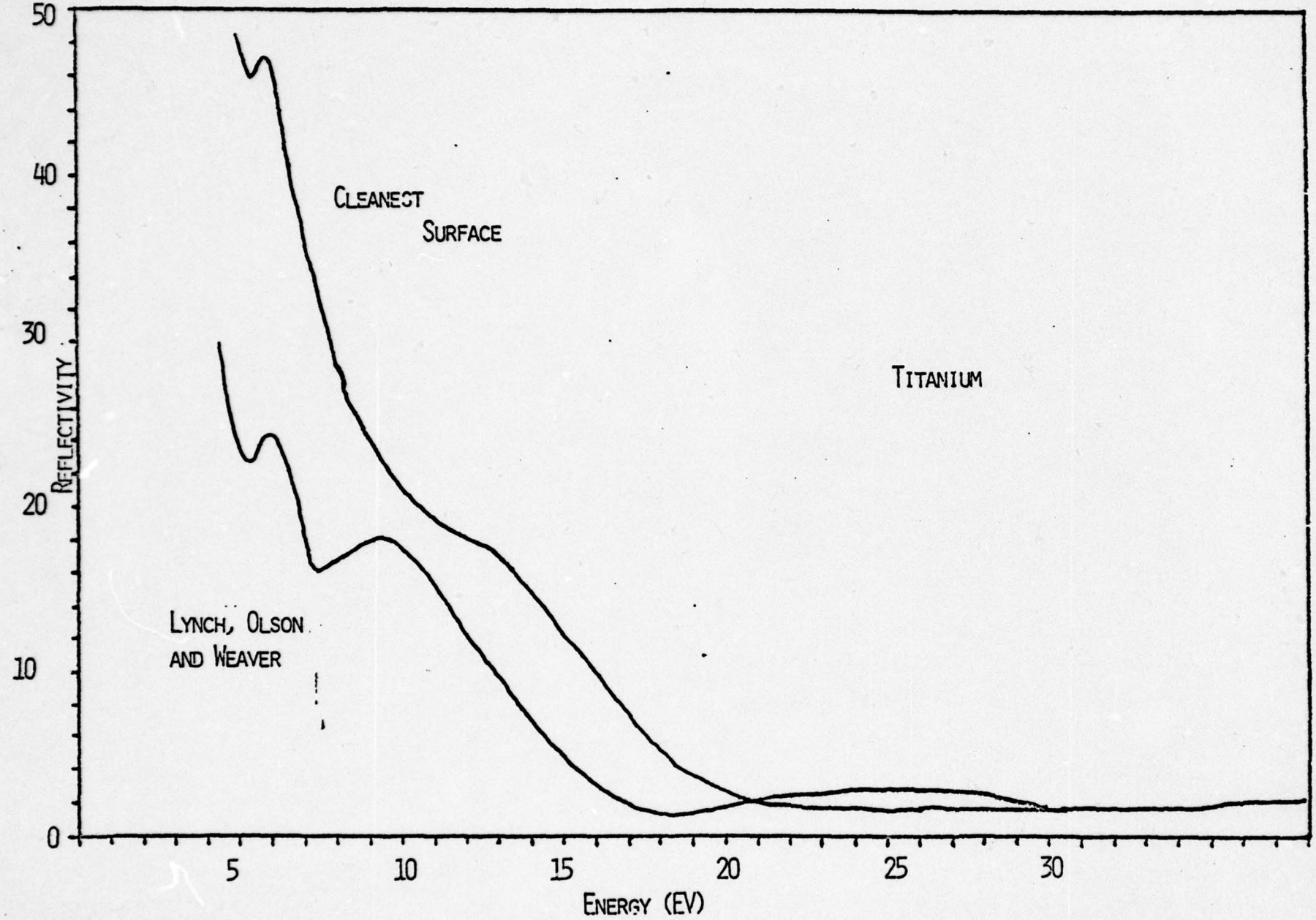
50
40
30
20
10
0
REFLECTIVITY
CLEANEST
SURFACE
TITANIUM
LYNCH, OLSON
AND WEAVER
5
10
15
20
25
30
ENERGY (EV)

Figure 6

surface spectra.

Figure 7 shows the reflectance spectra after successive oxygen bombardments with the build-up of the oxygen peak at about 10 eV, the movement to lower energy and build-up of the oxygen peak above 20 eV, and the reduction of the d-band structure between 5-7 eV. Note that although the bombardment builds an oxide much thicker than that on the initial surface, none of the spectra match the initial surface spectrum. In particular the peak at 10 eV remains fixed in energy even for the thick oxides, and does not move to lower energy as for the initial surface. However, the peak above 20 eV does move to lower energy and the d-band structure is reduced, these features being comparable to the initial surface structure. It is possible that during the oxygen bombardment regions of different oxide structure are formed on the surface. The predominant structure might be TiO-like, but with regions having TiO_2 structure. The reflectance spectrum would then show a combination of the features of these oxides. Some difficulties we have had in the Kramers-Kronig analysis of our data may also be due to this mixed structure. It is evident from the drastic reduction of the d-band structure in the 5-7 eV region, however, that as the oxide thickens the ultimate structure is TiO_2.

To further the identification of the oxide structure on the titanium surface, we have also made reflectance measurements on TiO_2 single crystals. The spectrum, presented in Figure 8, shows a peak at about 7.5 eV and a very broad structure extending from 12 to 25 eV with a maximum at about 18 eV. A shift to lower energy of the 10 eV structure in the earlier spectra is compatible with the formation of a TiO_2 phase, as indicated by the peak at about 7.5 eV. The peak at about 13.6 eV in Figure 8 is unexplained, but the position of the maximum at 18 eV again indicates the shift of the 25 eV peak to lower energy in the earlier spectrum may signal transition to a TiO_2 structure.

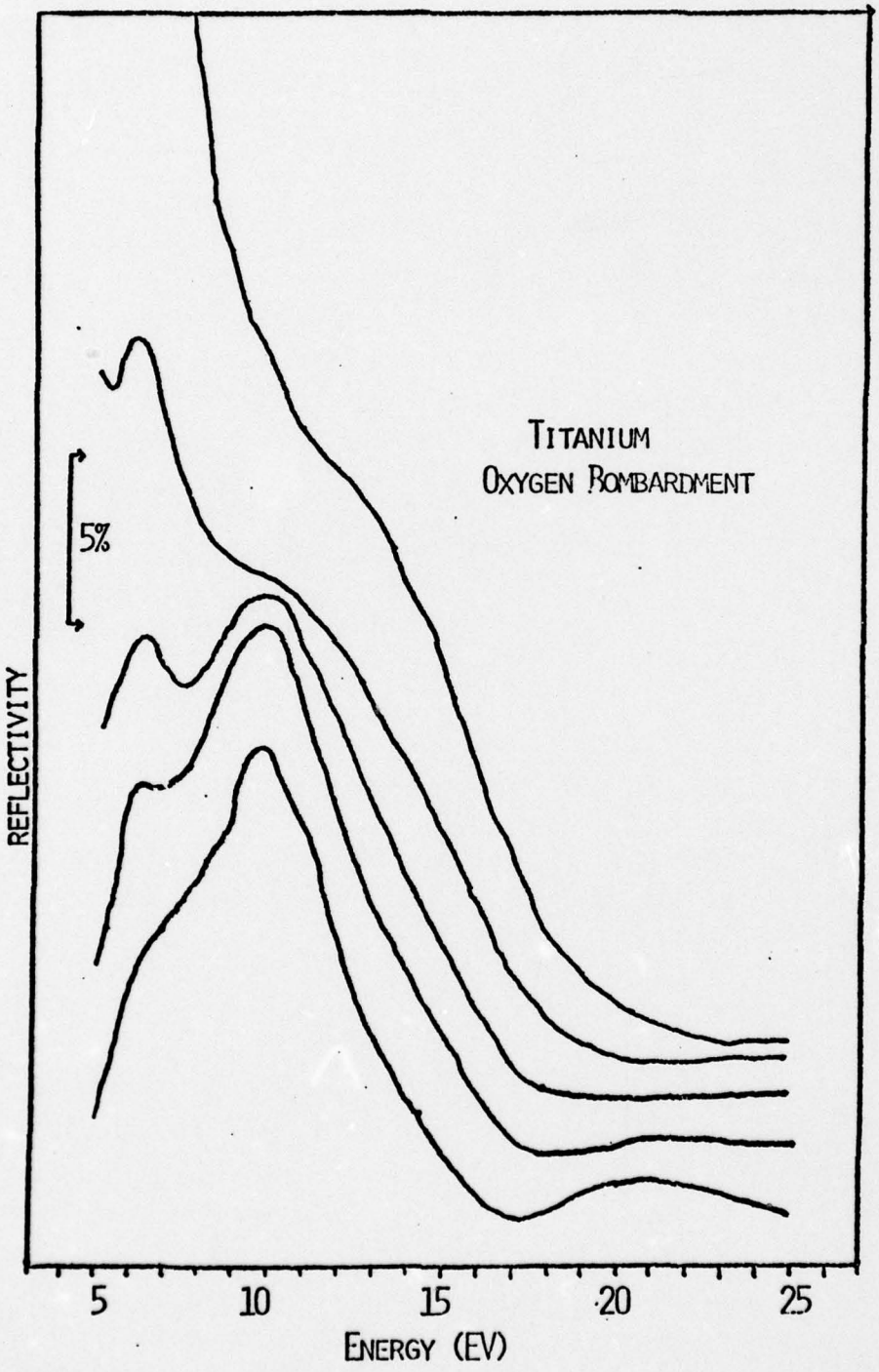
TITANIUM
OXYGEN BOMBARDMENT
5%
REFLECTIVITY
5
10
15
20
25
ENERGY (EV)

Figure 7.

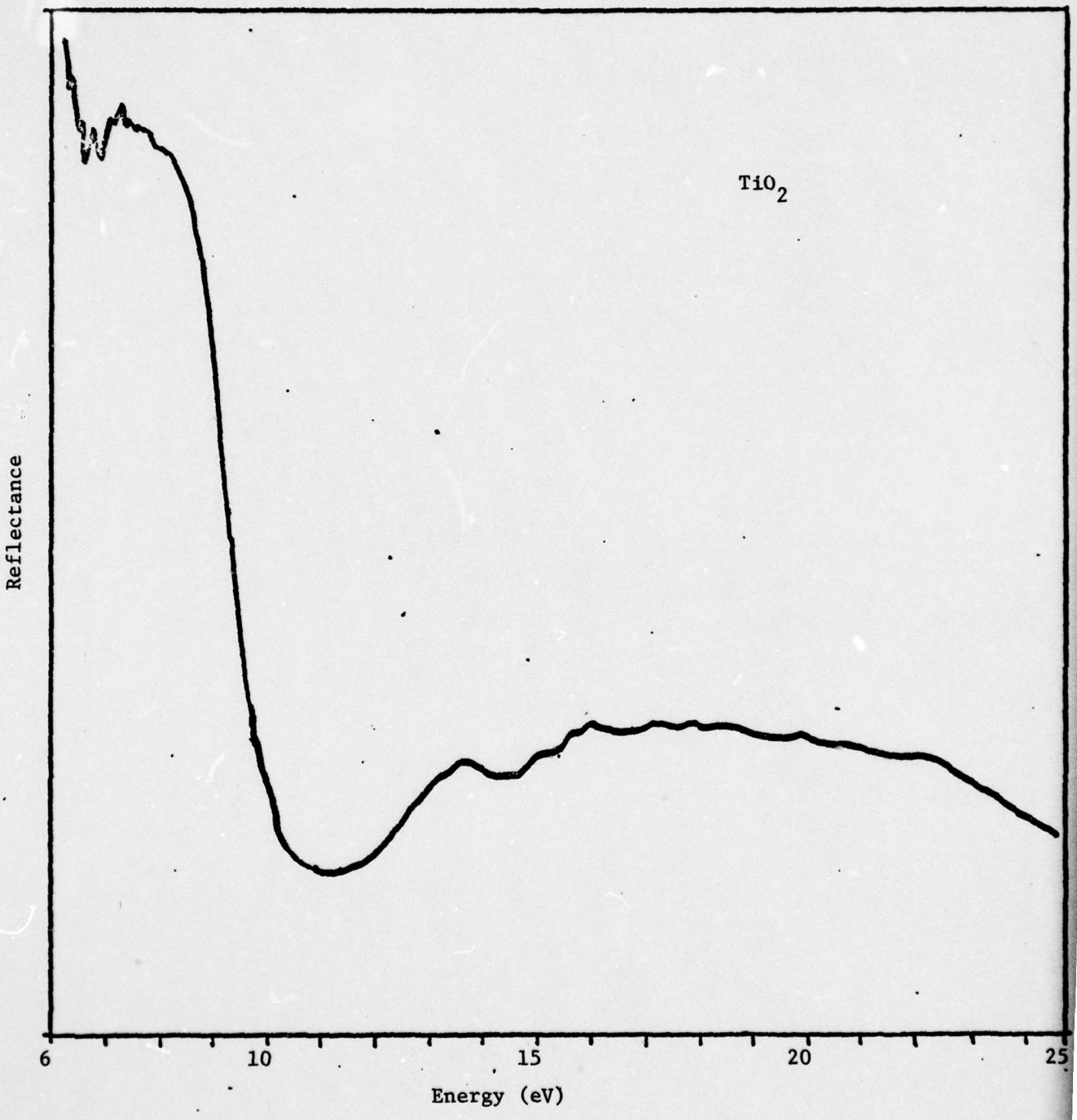

Figure 8

2. Auger spectra of the titanium-titanium oxide systems-

The Auger spectra of the initial surface (Figure 9) show a very strong oxygen peak. Using relative Auger sensitivities[10] we calculate the atomic ratio of oxygen to titanium to be 1.95 at the surface. Other identified impurities are sulfur (.04 S/Ti) and carbon (2.1). The carbon lineshape is that of free carbon rather than the carbide. After Ar sputtering (Figure10) we see that the oxygen ratio has dropped to .53 indicating less than a monolayer coverage. Carbon contamination has been reduced to 1.06 but the lineshape indicates a carbide presence, presumably TiC. Subsequent annealing of the sample at 700°C for 1 hour (Figure 11) reduces both the oxygen and carbon contamination to insignificant levels. A dramatic change in the titanium lineshape now shows the sample to be free of nitrogen, whose Auger transition at 379V was obscured by the Ti transitions at 383V and 387V.[11] The large sulfer peak (1.01) is produced by segregation from the bulk at high temperatures.[12] The concentration ratio suggests TiS as a surface layer. Bombarding the surface with 1 keV oxygen ions produces an oxide layer with an oxygen to titanium ratio of 1.3 suggesting an oxide mixture dominated by TiO.

3. Titanium - Aluminum Alloy -

Measurements were performed on a titanium-aluminum alloy having a one-to-one atomic ratio. The measurements were done identically to those performed on pure titanium. The Auger spectra (Figure 12) showed strong oxygen and carbon peaks in addition to the titanium and 51 eV aluminum peaks. The ratio of oxygen to Ti on the initial surface was 4.7, suggesting a mixture of Al_2O_3 and TiO_2 on the surface. The ratio of Ti to Al could not be accurately measured due to the large difference in sensitivity between the Ti and Al peaks.

The reflectivity spectrum (Figure 13) shows the dramatic change in reflectivity as the oxide layer is removed through Ar sputtering. The peak at 9 eV appeared at an intermediate stage in the cleaning, disappearing as the surface became

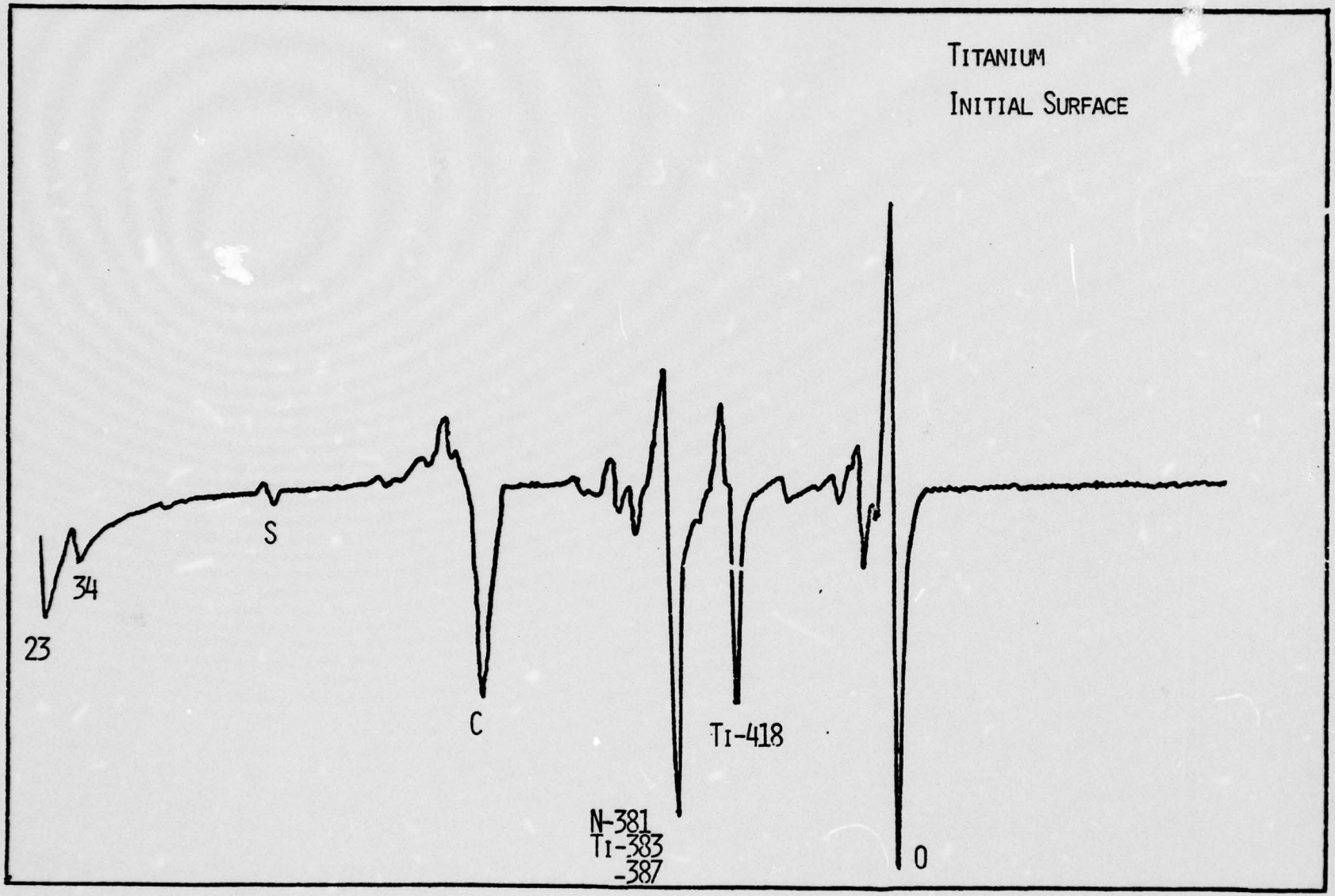

Figure 9 Auger Spectra of initial titanium surface

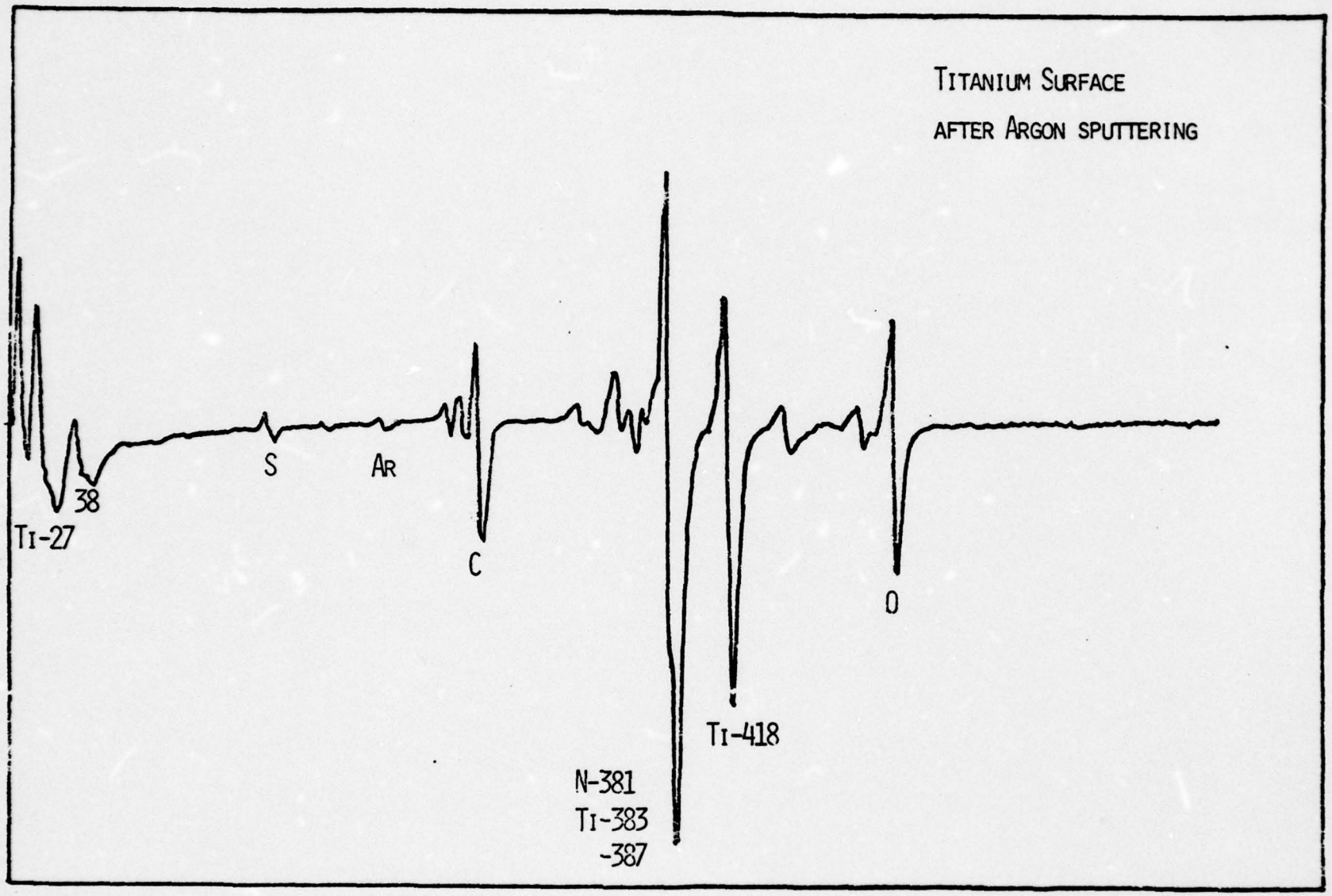

Figure 10 Auger spectra of titanium surface after Ar sputtering

cleaner; with the higher peak shifting to higher energy, finally disappearing. The behavior of the 9 eV peak is similar to that seen in the pure titanium at 6 eV. Bombarding the sample with oxygen ions grows an oxide layer with different optical characteristics from the initial surface. Figure 14 shows reflectivity for progressive stages of oxidation. Note that the 9 eV peak remains while the 7 eV peak disappears, with the high energy peak shifting to lower energy. Figure 15 compares the reflectivity of TiO_2 with oxidized Ti-Aℓ. The upper Ti-Aℓ curve was produced by oxygen ion bombardment while the lower curve was produced by heating Ti-Aℓ in oxygen.

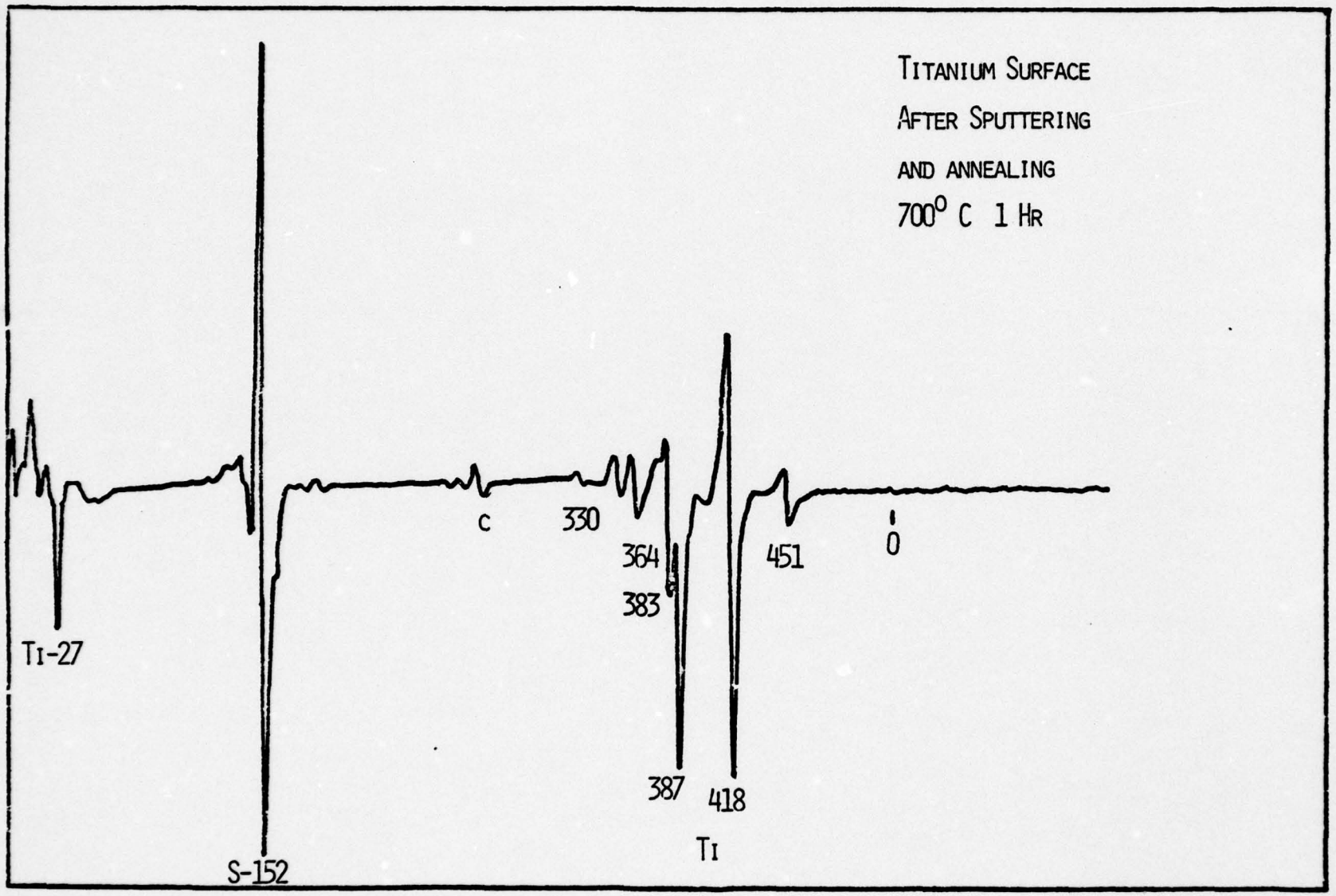

Figure 11 Titanium Auger spectra after Ar sputtering and annealing

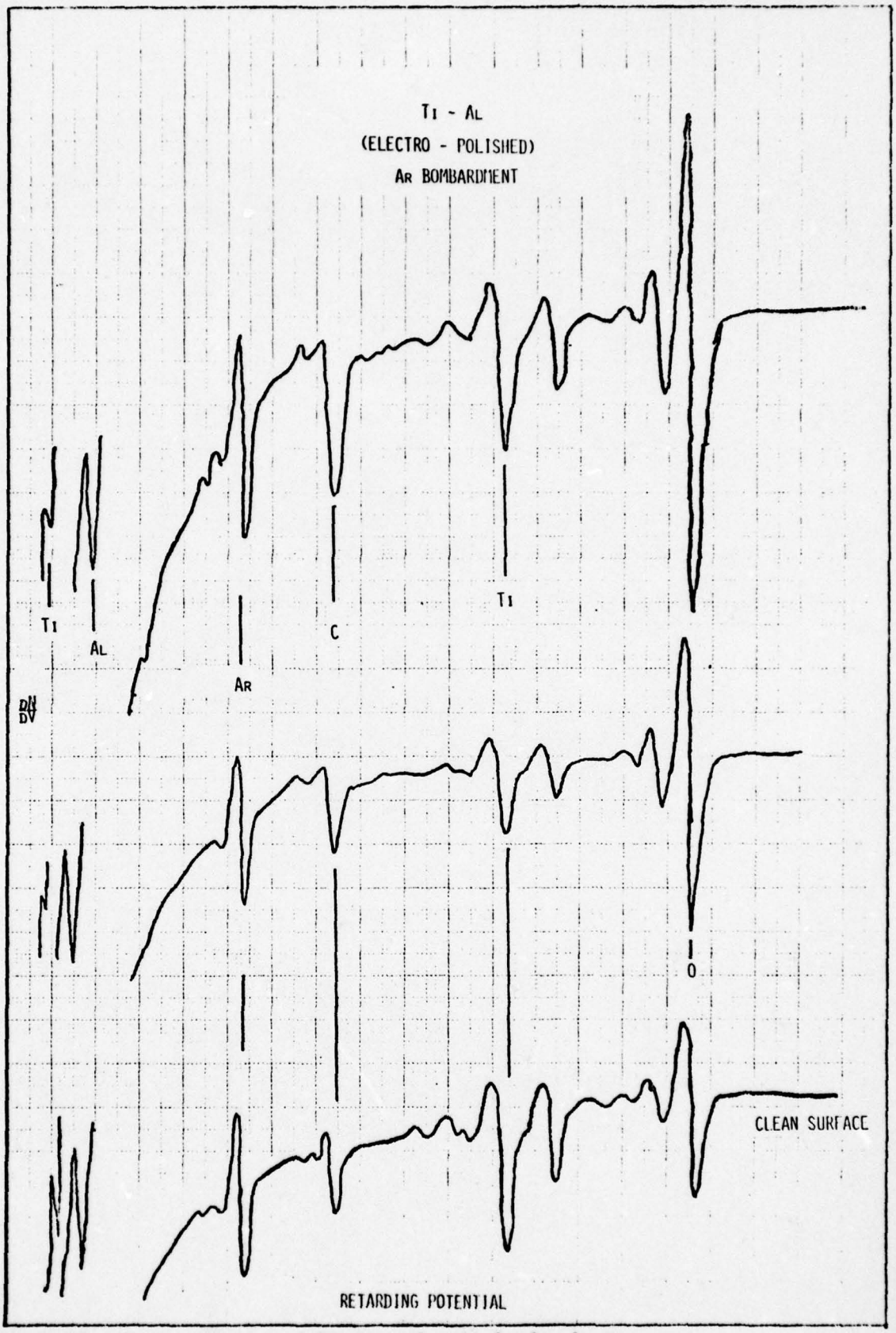

Figure 12 Auger spectra of Ti-Aℓ under Ar bombardment

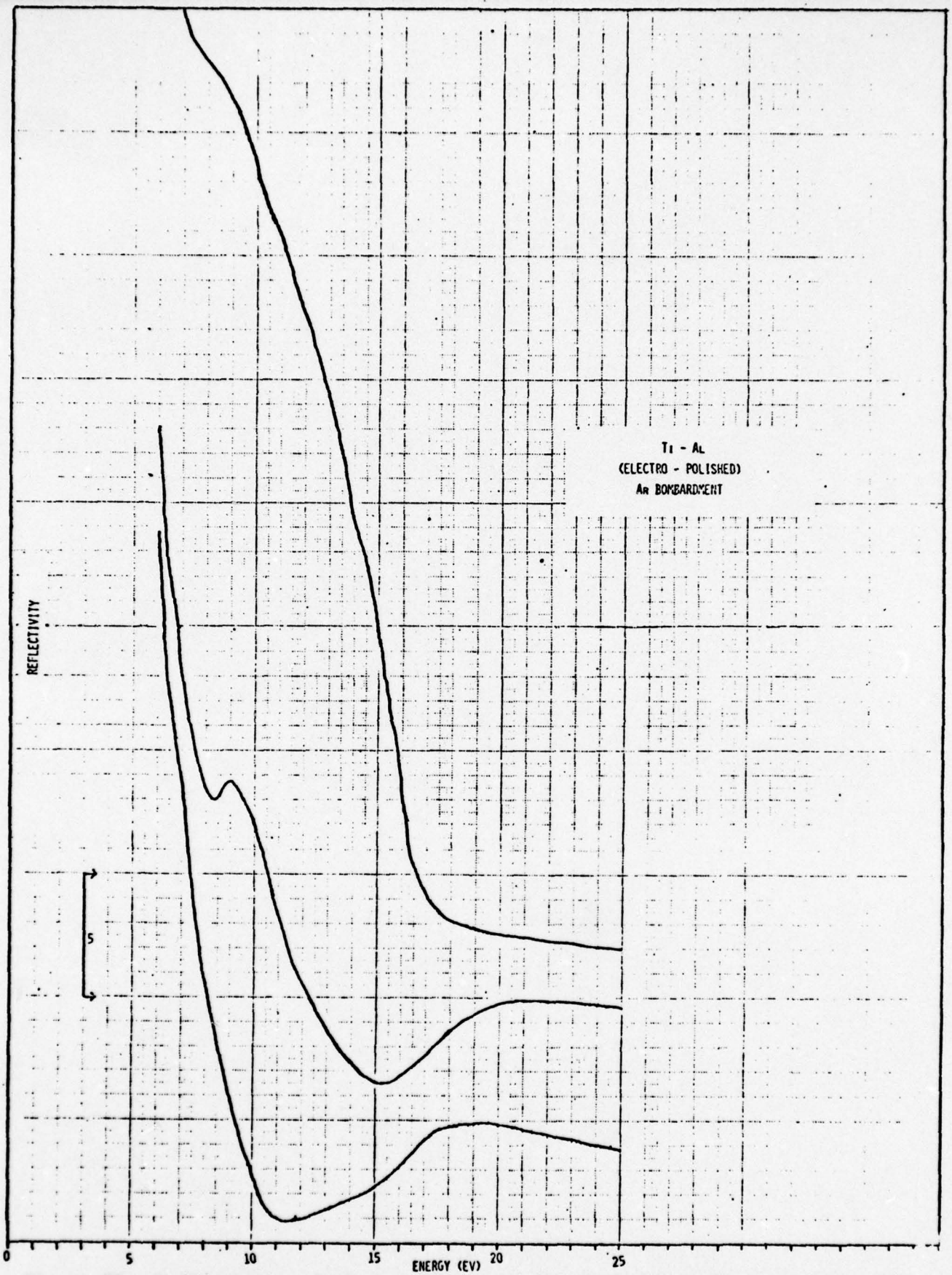

Figure 13 Reflectivity of Ti-Aℓ. Lower curve is initial surface. Curves above show reflectivity after successive periods of argon bombardment.

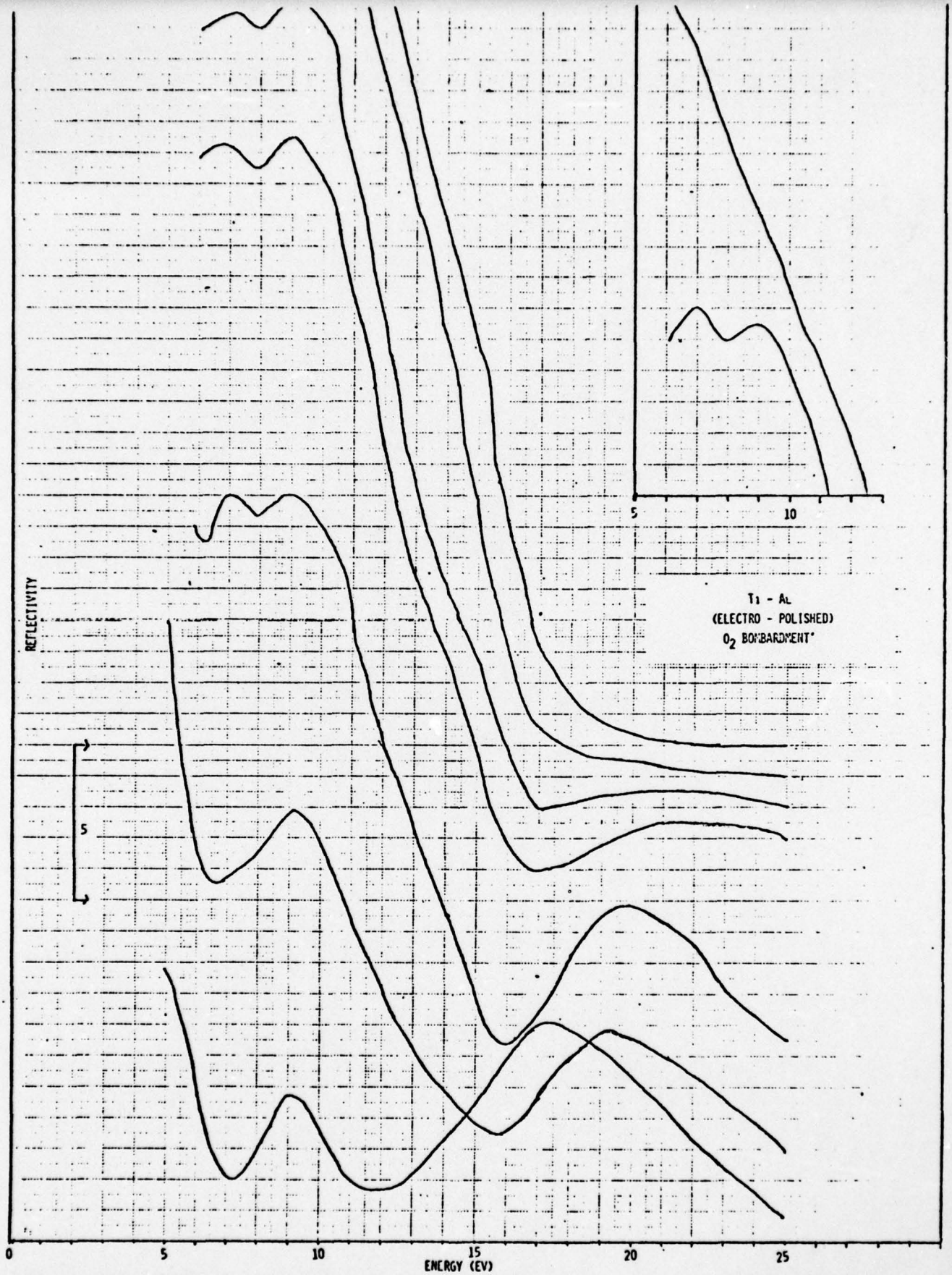

Figure 14 Reflectivity of Ti-Aℓ after successive periods of oxygen bombardment. Lower curve is most heavily oxidized.

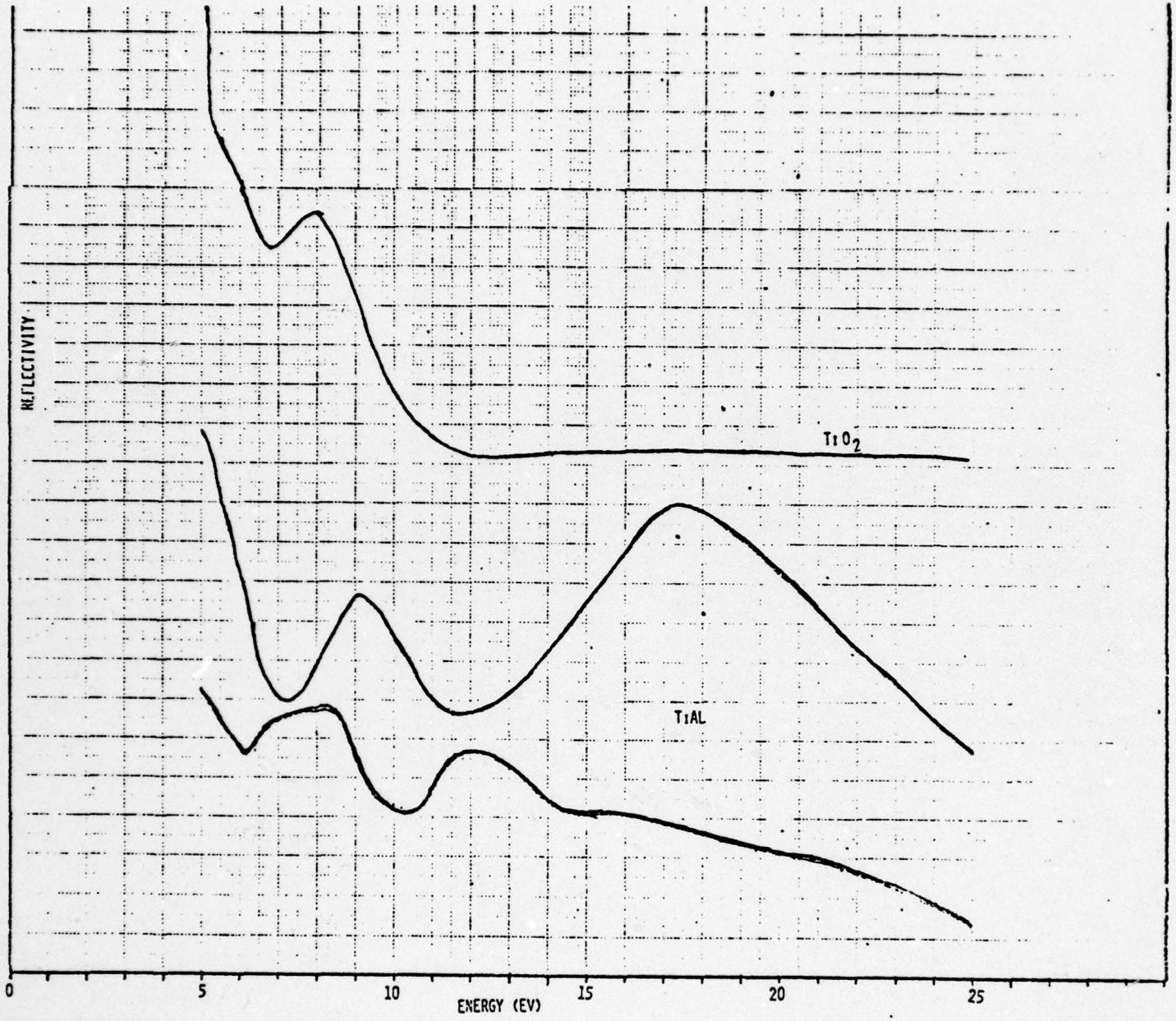

Figure 15 Comparison of reflectivity of two oxidized Ti-Aℓ samples with TiO_2 reflectivity

D. Optical Constants: Derivation and Analysis-

The real and imaginary parts of the complex index of refraction may be written

$$n = \frac{1 - r_o^2}{1 + r_o^2 - 2r_o \cos\theta} \tag{3}$$

$$k = \frac{2r_o \sin\theta}{1 + r_o^2 - 2r_o \cos\theta} \tag{4}$$

for normal incident light where $r_o^2 = R$ is the ratio of reflected to incident intensity and θ is the phase angle. If the reflected intensity is measured over a sufficient energy interval, the Kramers-Kronig (KK) relation

$$\theta(\omega_o) = \frac{-1}{2\pi} \int_o^\infty \frac{d \ln R}{d\omega} \ln \left| \frac{\omega + \omega_o}{\omega - \omega_o} \right| d\omega \tag{5}$$

may be used. A power law extrapolation $R(E) = R_o E^{-\gamma}$ has typically been used to describe the high energy tail of R(E) in Eq. (5). Since core-level excitations introduce additional structure in R(E) at higher energies, this extrapolation should not be assumed to give an accurate representation of the reflectivity. However, if the exponent γ is scaled so that the resulting n and k satisfy the sum rules given in Eqs. (1) and (2), good results are obtained in the measured energy range. This is especially true for the sum of Eq. (2), which shows a greater dependence on lower frequency optical behavior than does Eq. (1).

Once the complex refractive index is calculated, the complex dielectric constant may be constructed via the expression

$$\varepsilon_1 - i\varepsilon_2 = (n - ik)^2$$

The quantity $\varepsilon_2(\omega)$ gives the absorption spectrum of the system and therefore

describes the excitation structure. If one neglects final state effects introduced by the interaction of the excited electron with its hole and also neglects any intraband contributions, then $\varepsilon_2(\omega)$ has the form

$$\varepsilon_2(\omega) \sim \frac{1}{\omega^2} \sum_{n,s} \sum_{BZ} \delta(\omega_{n,s}(\vec{k}) - \omega) |M_{n,s}(\vec{k})|^2 \, d^3k \qquad (6)$$

The subscripts n and s refer to filled and unfilled bands respectively, and $\omega_{n,s}(\vec{k}) = \omega_n(\vec{k}) - \omega_s(\vec{k})$. The momentum matrix element $M_{n,s}(\vec{k})$ between states in bands n and s is nearly constants for bands with little dispersion. Then

$$\varepsilon_2(\omega) \sim \frac{1}{\omega^2} \, N_J(\omega) \qquad (7)$$

where $N_J(\omega)$ is the joint density of states.

The various spectrum segments taken from the discharge source and from the synchrotron had to be scaled to provide a smooth curve. Curves requiring the least amount of scaling were obtained using a segment of the data from the synchrotron as a standard, and this procedure was used throughout. However, a variation of several percent could occur in the magnitude of the reflectance curve depending on which segment was used for scaling. To study the effect of this change in magnitude on the optical constants, we calculated the optical constants of the oxidized titanium surface for two extreme cases of scaling. Figure 16 compares the joint density of states, calculated using Eq. (7), for these two scalings. It is seen that the spectral shapes compare well up to about 18 eV with peak shifts of no more than a few percent, but that the final peak at 22-25 eV shifts by 3-4 eV, as is to be expected since this peak is at the edge of the data. Thus one should keep in mind in what follows that magnitudes of the optical constants may not be precise, but that the positions and relative magnitudes of peaks are reliable, except, possibly, for peaks above 20 eV. Unfortunately we were not able to make a KK analysis of the Ti-Aℓ

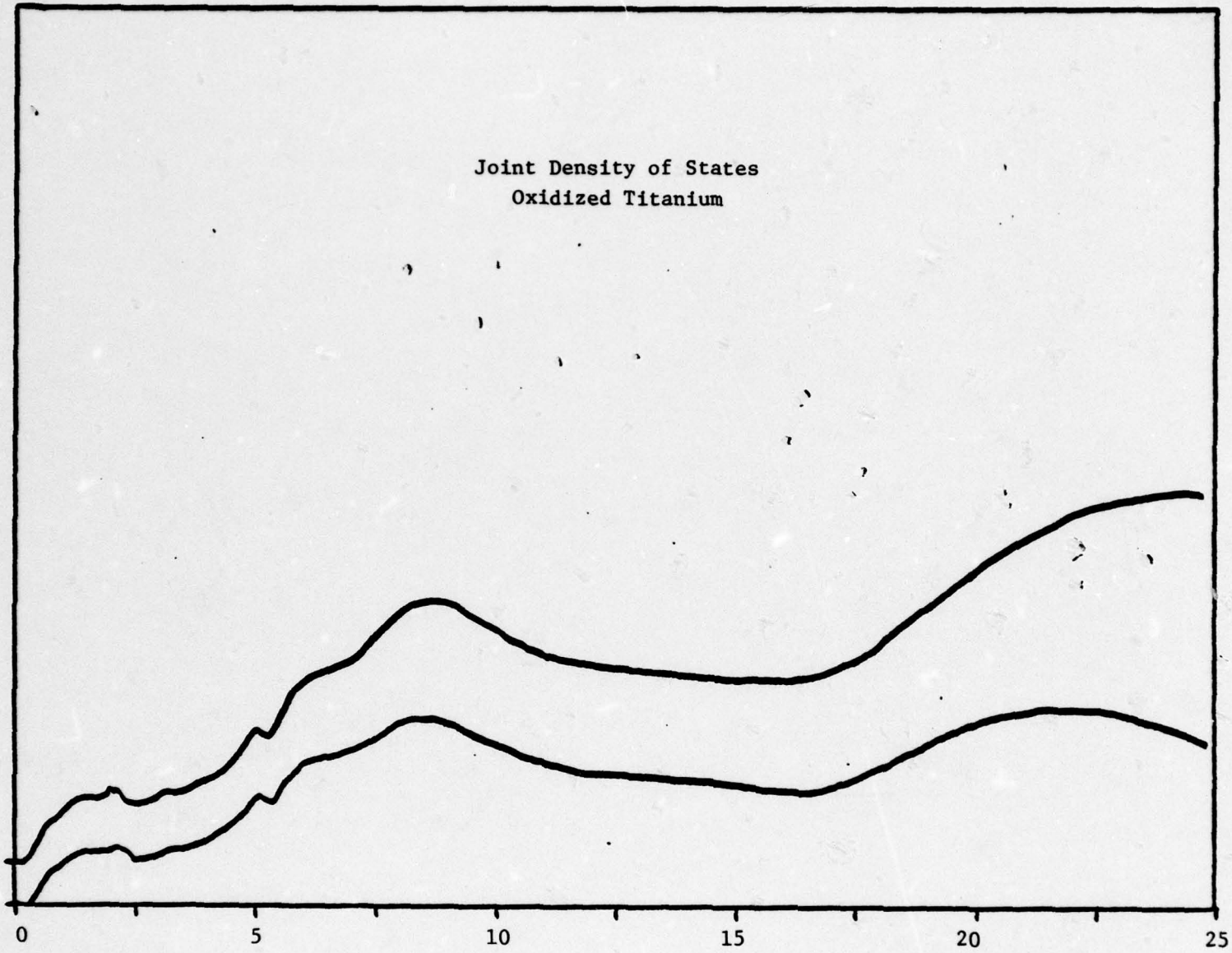
Joint Density of States
Oxidized Titanium
0
5
10
15
20
25
Energy (eV)

Figure 16

data due to incomplete reflectivity measurements in the region below 5 eV.

The KK analyzed spectra of ε_1 and ε_2 for the clean and oxidized titanium surfaces are shown in Figure 17. The changes in structure among the ε_2 spectra are in most cases similar to the changes in the reflectivity spectra. Note, however, that the 10 eV peak moves much less in going from the oxidized to initial surface ε_2 spectrum than it does in the comparable reflectivity spectra. The structure is also less pronounced in the ε_2 spectra than the corresponding structure in the reflectivity data.

To gain a more detailed understanding of the oxide structure, we have obtained the energy bands for TiO calculated recently by Jennison and Kunz.[13] These ab-initio self-consistent field energy bands calculated within the local orbital model give good agreement with experimental TiO XPS valence spectra.[14] We have used these bands to construct the joint density of states in the optical region from 0 to 2 Ryd. The calculated density of states in Figure 18 has peak structure which compares well with the experimentally derived density of states depicted in the topmost curve of Figure 16. In Table I we present a comparison of peak maxima among our calculated and experimentally derived densities of states and Lynch's ε_2 data.[7] It is seen that the calculated structure is in general agreement with our experimental data as well as the lower energy part of Lynch's data. A check of the contributions to the peak structure centered at about 9 eV in Figure 18 indicates that states with p-like symmetry dominate the initial state. The peak at about 27 eV is mostly oxygen 2s in the initial state. This peak is higher in energy than the corresponding peaks in Figure 16 and all other oxide ε_2 data. Since the XPS spectrum also shows an O2s peak[14] at lower energy than the corresponding peak in the energy band density of states, this shift is at least partly due to final state relaxation in the more localized O2s band, although particle-hole interactions probably produce a further shift to lower energy in the optical spectrum.

Table I. Comparison of peak maxima from the calculated and experimentally derived joint densities of states and Lynch's ε_2 data. All energies are in eV.

Calculated[a]	Experiment[b]	Lynch *et al*[c]
3.28	3.32	3.2
5.44	5.20	5.6
6.34	6.45 (shoulder)	
9.40 (central maximum)	8.78	8.2
27.3	24.5	23.8

a. See Figure 17

b. See Figure 15

c. Ref. 7

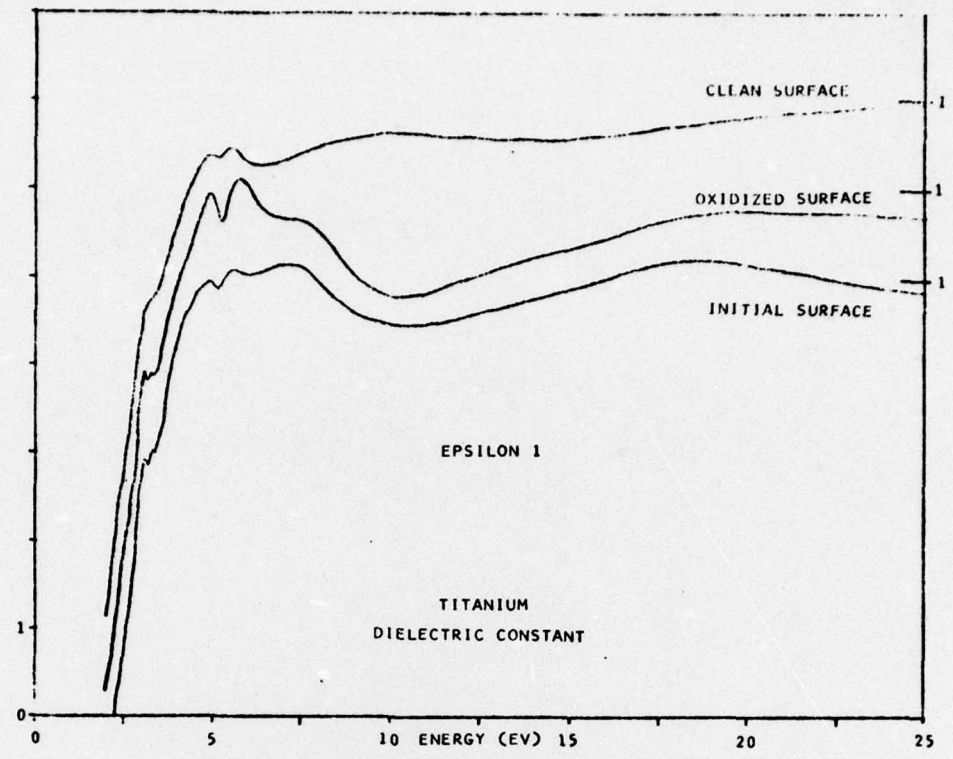
CLEAN SURFACE
OXIDIZED SURFACE
INITIAL SURFACE
1
1
1
EPSILON 1
TITANIUM
DIELECTRIC CONSTANT
1
0
0
5
10 ENERGY (EV) 15
20
25

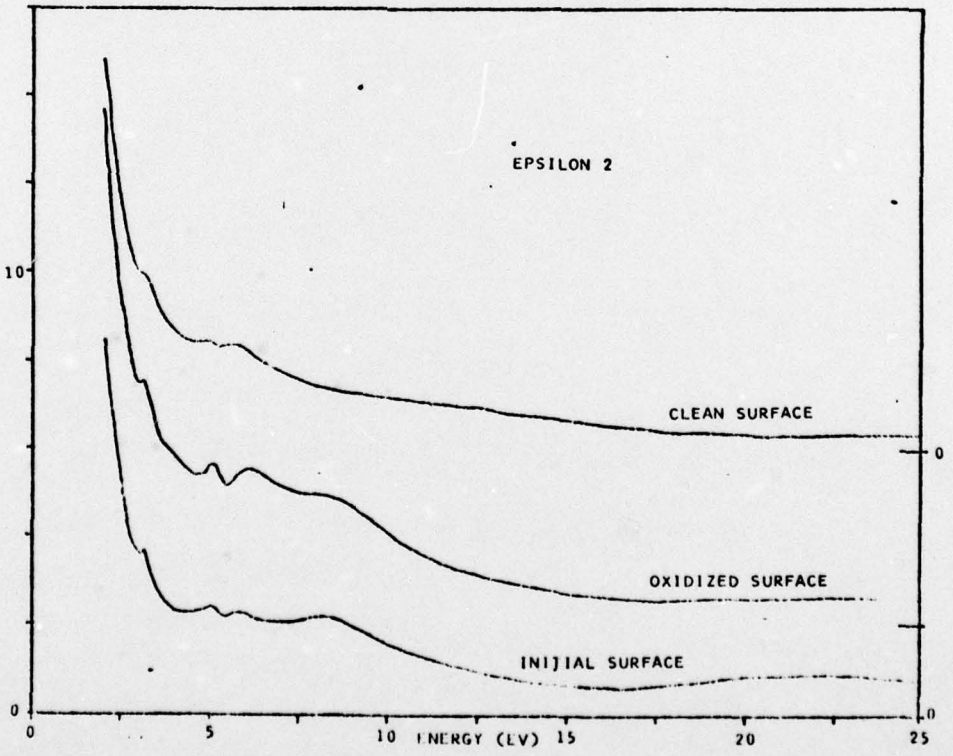
EPSILON 2
10
CLEAN SURFACE
OXIDIZED SURFACE
INITIAL SURFACE
0
0
0
0
5
10 ENERGY (EV) 15
20
25

Figure 17

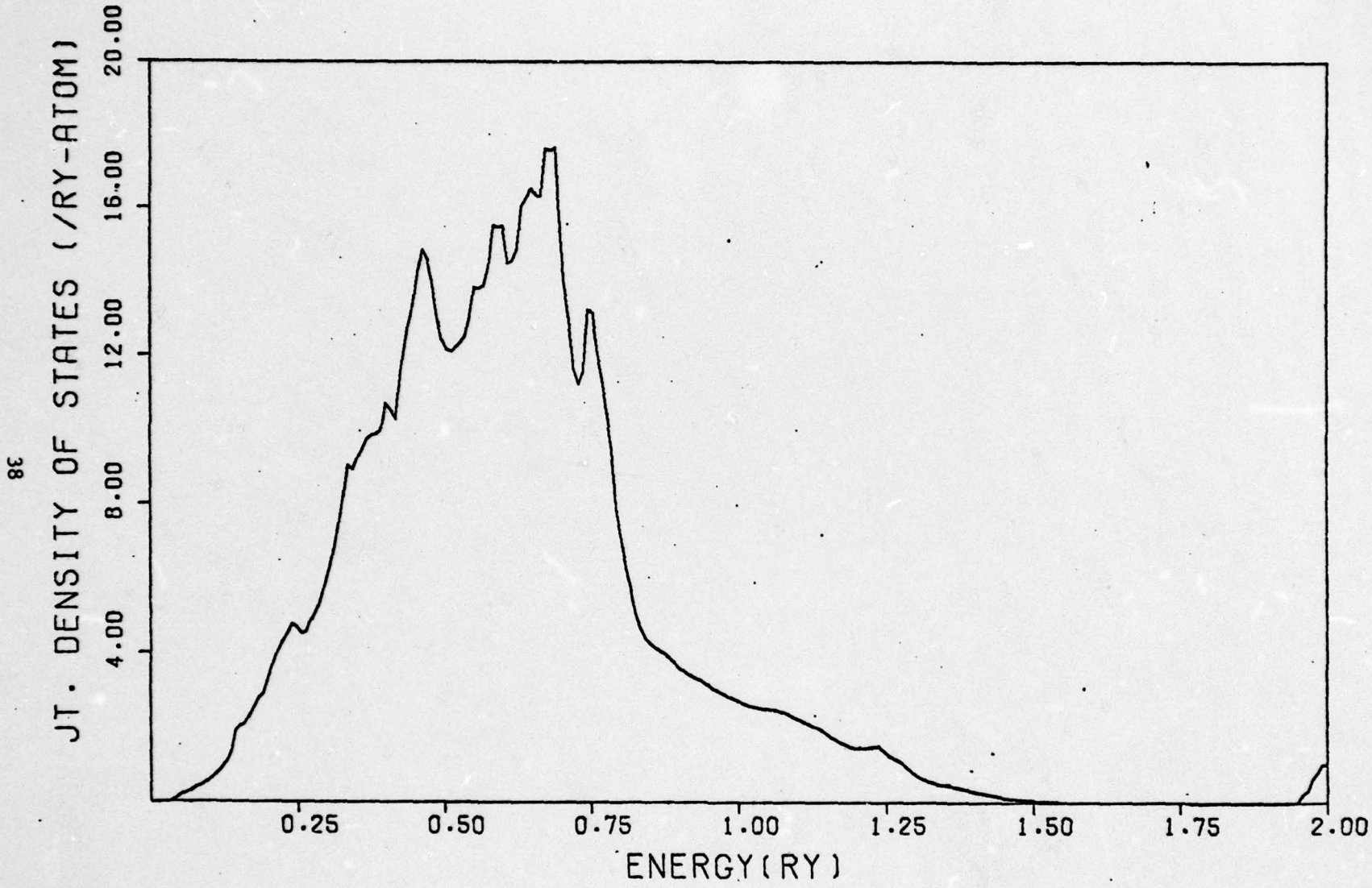

Figure 18 Joint density of states calculated using energy bands of Jennison and Kunz.[13]

E. Conclusions

The reflectivity of titanium surfaces undergoes significant changes as oxides are formed. Careful cleaning monitored by Auger spectroscopy is necessary to insure a clean Ti surface and several previous Ti reflectivity measurements show significant structure due to residual oxides. Cycles of oxygen bombardment followed by argon sputtering yield reproducible reflectivity spectra. Ti-O Auger peak height ratios indicate the initial oxide on the surface is TiO_2 but that the oxide produced on the clean surface by oxygen bombardment is TiO - like. Further oxygen bombardment produces a trend toward a TiO_2 structure. This viewpoint is supported by reflectivity measurements we have made on single crystal TiO_2.

The Kramers Kronig analysis of the reflectivity data produces optical constants with accurate spectral shapes. However, the structure in ε_2 is less pronounced than in the reflectivity spectra, and the shifts in peak positions as the oxide is formed are less. The joint density of states calculated using self-consistent TiO energy bands is in general agreement with the joint density of states from our oxygen bombarded surface. This result is compatible with our notion that this oxide film is predominantly TiO, but no clear-cut assignment of oxide structure is possible on the basis of either the calculated or experimentally derived optical constants.

The reflectivity of the Ti-Aℓ surface also undergoes significant changes as oxides are formed. Here the resultant structure is less easily analyzed than for the Ti surface, but it reflects changes in oxide structure. The oxygen Auger structure suggests a mixture of $Aℓ_2O_3$ and Ti oxide on the surface, and this result is substantiated by the appearance of peak structure in the oxide reflectivity which correspond to peaks in the Ti oxide reflectivity and other structures which seem to be due to the Aℓ oxide.

For the titanium-titanium oxide surfaces, the reflectivity is more sensitive

to changes in oxide structure than are the optical constants. Regions of particular sensitivty are peaks at about 8-10 eV and above 20 eV in the oxide spectra and to a lesser extent the structure from 5 to 6 eV. Measurements of the changes in magnitude and the relative magnitudes of the reflectivity in these regions would yield information on the oxide structure. Additional measurements, for example core-valence-valence Auger spectra or LEED, are in order to complete the understanding of the oxide formation process.

F. References

1. H.W. Ellis and J.R. Stevenson, J. Applied Physics 46, 306 (1975).

2. F.L. McCrackin, Nat'l Bur. Std. U.S. Tech. Note 479, U.S. Govt. Printing Office, Washington, D.C. (1969).

3. S.S. So, Surface Sci 56, 97 (1976).

4. M.W. Ribarsky and E.J. Scheibner, J. Applied Physics, to be published.

5. L.R. Kahn, P. Baybutt, and D.G. Truhlar, J. Chem. Phys. 65, 3826 (1976).

6. C.F. Melius, J.W. Moskowitz, A.P. Mortola and M.B. Baillie, Surf. Sci. 59, 279 (1976).

7. D.W. Lynch and C.G. Olson, Phys. Rev. B 11, 3617 (1975).

8. David W. Fischer, J. Appl. Phys. 41, 3561 (1970).

9. S. Hüfner and G.K. Wertheim, Phys. Rev. B 8, 4857 (1973).

10. Handbook of Auger Spectroscopy (Second Edition) Davis et al., Physical Electronics, Ind. 1976.

11. H.D. Shih, K.O. Legg, and F. Jona: Surface Sci, 54, 355-364 (1976).

12. T. Smith, J. of Op. Society of A. 62, 6, 774-780 (1972).

13. D.R. Jennison and A.B. Kunz, Phys. Rev. Lett. 39, 418 (1977).

14. K. Ichikawa, O. Terasaki and T. Sagawa, J. Phys. Soc. Japan 36, 706 (1974).

III. Professional Personnel

The following individuals have participated in the research described above.

1.	Dr. James R. Stevenson	Principal Investigator
2.	Dr. Keith Legg	Research Scientist
3.	Dr. William Ribarsky	Research Scientist
4.	Mr. Bruce Biskey	Graduate Student
5.	Mr. Sam Formby	Graduate Student
6.	Mr. James Larsen	Graduate Student
7.	Mr. Bill Wall	Graduate Student
8.	Mr. Ron Yanda	Undergraduate Student

In addition to the personnel named above:

Dr. Victor Krevs and Dr. Tristanas Budinas from the USSR each spent a year at Georgia Tech in our laboratory. Although they were not involved in the research described above, they did occasionally make use of some of the equipment previously described.

IV. Communications

The following communications have taken place or they are being planned as a result of the research described.

A. Papers Presented

1. "Optical Reflectivity and Auger Spectroscopy of Ti and Ti-Aℓ with W. Wall, J. Larsen, and W. Ribarsky, Physical Sciences Laboratory, University of Wisconsin, October 20, 1975.

2. "Optical Reflectivity and Auger Spectroscopy of Ti and Ti-Aℓ Alloys," with W. Wall, J. Larsen, and W. Ribarsky, Southeastern Section of the American Physical Society, Auburn, Alabama, November 14, 1975.

3. "Optical Properties of Ti and Ti-Aℓ Alloys from 2 eV to 50 eV," with W. Wall and J. Larsen, Bull. Am. Phys. Soc. 21, 319 (1976).

4. "Optical Properties of the $Hg_{(1-x)}$ Mn_x Te Solid Solutions ($0 < x \leq .11$)," with V.E. Krevs and W.E. Wall, Bull. Am. Phys. Soc., 21, 366 (1976).

5. "Optical Reflectivity and Auger Spectroscopy of Titanium Surfaces Bombarded with Nitrogen Ions" with W. Wall and J. Larsen, Ninth Annual Synchrotron Radiation Users Group Conference, October 25, 1976.

6. "Optical Reflectivity and Auger Spectroscopy of Titanium Surfaces with Controlled Exposures to Oxygen and Nitrogen," with W. Wall, J. Larsen, K. Legg, and Vth. International Conference on Vacuum Ultraviolet Radiation Physics, Montpellier, France, September, 1977.

7. "On Line Optical and Auger Data Acquisition," with W. Wall, Synchrotron Radiation Instrumentation and Developments Conference, Orsay, France, September, 1977.

B. Papers Accepted for Publication

"Optical Reflectivity and Auger Spectroscopy of Titanium Surfaces with Controlled Exposures to Oxygen and Nitrogen," with W. Wall, J. Larsen, K. Legg, and W. Ribarsky, accepted for publication in the Conference Book on the Vth. International Conference on Vacuum Ultraviolet Radiation Physics, Montpellier, France 1977.

"On line Optical and Auger Data Acquisition" with W. Wall, accepted for publication in Nuclear Instruments and Methods as a contribution to Synchrotron Radiation Instrumentation and Developments Conference, Orsay, France 1977.

C. Papers in Preparation

1. "Optical Reflectivity and Auger Spectroscopy of Titanium Surfaces" with W. Wall, W. Ribarsky and K. Legg

D. Ph.D. Thesis

1. W. Wall, "Optical Reflectivity and Auger Spectroscopy of Titanium Surfaces, anticipated March 1978.

E. Research Group Interactions

1. Physical Sciences Laboratory, University of Wisconsin, Madison Wisconsin
2. E. Koch and B. Sonntag, F-41 Group DESY Hamburg, W. Germany
3. T.C. Collins, AFOSR, Bolling AFB, Washington
4. D.W. Lynch, Physics Dept., Iowa State Univ.
5. E.T. Arakawa, Health Physics Division, Oak Ridge National Laboratory
6. Brian A. Manty, Pratt and Whitney Aircroft
7. E. Palik, U.S. Naval Research Laboratory
8. A.B. Kunz, Physics Department, University of Illinois- Urbana
9. D.R. Jennison, Sandia Laboratories, Albuquerque, New Mexico.
10. Frank Tobin, Chemistry Dept., Illinois Institute of Technology, Chicago, Illinois.